



ELSEVIER

Journal of Physics and Chemistry of Solids 64 (2003) 863–872

JOURNAL OF  
PHYSICS AND CHEMISTRY  
OF SOLIDS

[www.elsevier.com/locate/jpcs](http://www.elsevier.com/locate/jpcs)

# Instability of higher-energy phases in simple and transition metals

L.G. Wang<sup>a,\*</sup>, M. Šob<sup>a</sup>, Zhenyu Zhang<sup>b,c</sup>

<sup>a</sup>*Institute of Physics of Materials, Academy of Sciences of the Czech Republic, Žitkova 22, CZ-616 62 Brno, Czech Republic*

<sup>b</sup>*Solid State Division, Oak Ridge National Laboratory, Oak Ridge, TN 37831, USA*

<sup>c</sup>*Department of Physics, University of Tennessee, Knoxville, TN 37996, USA*

Received 1 March 2002; accepted 3 October 2002

## Abstract

We perform full-potential first-principles total energy calculations for several simple and transition metals along three distinct phase transformation paths, i.e. the tetragonal, trigonal and hexagonal paths. Our results show that higher-energy phases, such as the bcc structure for Al, Cu and Ti and the fcc structure for Nb, Mo, Ta and W, are always unstable with respect to one or more of transformation modes. Some local minima along the total energy profiles are found to correspond to the structures not dictated by the symmetry. We discuss the most interesting problem why a higher-energy phase may be stabilized in a pseudomorphic film.

© 2003 Elsevier Science Ltd. All rights reserved.

**Keywords:** A. Metal; C. Ab initio calculations; D. Phase transition; Instability; Pseudomorphic films

## 1. Introduction

Heteroepitaxial films have attracted much interest because of their applications in optical and electronic devices. A pseudomorphic film may be strained strongly because, in the coherent case, it has to match the lattice of the substrate. Therefore, some higher-energy phases, which are not normally encountered in bulk form, may be observed in heteroepitaxial films. Indeed, experiments have indicated that the bcc Cu phase exists in the pseudomorphic Cu films grown on the {001} surfaces of Pd, Pt, Ag, and Fe [1–7] and in multilayers of Cu with Nb [8–10]. (The structure of the pseudomorphic Cu films on the Pd{001} and Pt{001} substrates is also considered to be the deformed fcc [11,12]) The fcc Co phase has been reported in thin Co films on the Cu{001} and Cu{111} substrates [13]. Hcp Al and fcc Ti have been also observed in Ti/Al multilayered thin films [14]. Theoretically, Marcus and Jona [15] found a criterion for identifying the phase structure in pseudomorphic films

based on the stability analysis using ab initio electronic structure total energy calculations. However, the nature of the existence of higher-energy phases in pseudomorphic films is not yet completely understood [16].

To predict structural properties of solids, ab initio (first-principles) electronic structure calculations within the framework of density-functional theory (DFT) [17,18] employing the local-density approximation (LDA) or the generalized gradient approximation (GGA) have been performed widely [5,12,16,19–27]. In such studies, the atomic numbers of the constituent atoms and some structural information are the only input data. In contrast to the empirical methods, where adjustable parameters are usually fitted to the properties of the ground state, ab initio calculations can be applied reliably also to the atomic configurations far from the ground state.

In the present paper, we study systematically the total energy profiles of simple and transition metals along three distinct transformation paths using a high-precision full-potential linearized augmented plane wave (FLAPW) method [28]. These transformation paths connect some higher-symmetry structures as special cases (Section 2), and are characterized by a single parameter  $p$ . The higher-symmetry structures occurring along a transformation path

\* Corresponding author. Present Address: National Renewable Energy Laboratory, 1617 Cole Blvd, Golden, CO 80401, USA. Tel.: +1-303-384-6409; fax: +1-303-384-6432.

E-mail address: [lwang@nrel.gov](mailto:lwang@nrel.gov) (L.G. Wang).

correspond to extreme points. We find that the higher-energy phases, such as bcc structure for Al, Cu and Ti and fcc structure for Nb, Mo, Ta and W, often correspond to a maximum of the total energy and, therefore, are unstable with respect to certain transformation modes. For the metals studied, a bct structure corresponding to a local minimum of the total energy profile along the tetragonal path, which is not dictated by the symmetry, is observed. Similarly, there exists an orthorhombic structure corresponding to a local energy minimum along the hexagonal path. We suggest that the stability of higher-energy phases in pseudomorphic films is due to the bulk stability of the substrate material, rather than surface and/or interface effects as usually believed.

## 2. Theoretical approach and calculation details

### 2.1. The calculation method

In the FLAPW method, the basis functions inside the spheres centered at atomic sites are linear combinations of radial wavefunctions and their energy derivatives, and in the interstitial region they are represented by a plane wave expansion. Thus no shape approximations are made to the charge density and potential. We employ the WIEN97 code developed by Blaha et al. [28]. The exchange–correlation potential is treated within the LDA; we use the Perdew and Wang 92 scheme [29] reparameterizing the Ceperly–Alder data [30]. We use a cut-off of  $R_{\text{mt}}K_{\text{max}} = 8$  for plane waves (for the definition see Ref. [28]) and of 225 Ry for star functions describing the wave functions, the charge density and potential in the interstitial region. The muffin-tin radii in our calculations are set to 2.20 au (Al), 2.00 au (Cu), 2.46 au (Ti), 2.15 au (Fe), 2.30 au (Nb), 2.35 au (Mo), 2.20 au (Ta), and 2.37 au (W). The total energy calculations for the tetragonal and trigonal transformation paths are performed with 4500  $k$ -points in the full Brillouin zone (BZ); for the hexagonal transformation path, 1125  $k$ -points are used because a supercell including four atoms (i.e. four times more than that for the other two transformation paths) is employed.

### 2.2. Phase transformation paths

We study the total energy profiles along the tetragonal, trigonal and hexagonal transformation paths. These transformation paths have been described and studied in many previous papers [5,24–27,31–36]. Our tetragonal and trigonal paths are the same as previous ones [5,24–27,32–36]. However, our hexagonal path in which the intermediate structures between the bcc and hcp structures are interpolated linearly [32] is different from that used by Craievich et al. [25] and by Wentzcovitch and Cohen [31]. All transformation paths employed in this work may be described by a single parameter,  $p$ . Here we give only a short

characterization of these paths; a detailed description is given in Ref. [32].

The tetragonal transformation path, also called the Bain deformation path, is generally considered to be the simplest continuous path between the bcc and fcc lattices in elemental solids. Starting from the bcc lattice and selecting the [001] direction as the  $c$ -axis, this path corresponds to the continuous change of the  $c/a$  ratio, where  $a$  is the lattice parameter in the [100] and [010] directions. The volume per atom is usually constant along the path. The parameter  $p$  is equal to the  $c/a$  ratio and, in the case of an elemental solid  $p = 1$  for the bcc lattice and  $p = \sqrt{2}$  for the fcc lattice, represented as a body-centered tetragonal (bct) lattice with lattice parameters  $c$  and  $a$ . As a result of this transformation, the (100) plane in the bcc lattice becomes the (110) plane of the fcc lattice.

Starting from the bcc lattice, the trigonal path corresponds to the uniaxial deformation along the [111] axis while keeping the atomic volume fixed. In the case of an elemental solid this path connects three cubic structures, namely the bcc, simple cubic (sc) and fcc structures, and the parameter  $p$  of the path is defined to be again the  $c/a$  ratio where  $c$  is the length of a line segment in the lattice along the [111] direction and  $a$  is the length of a line segment measured along any perpendicular direction. Again, we set  $p = 1$  for the bcc structure; then  $p = 2$  for sc and  $p = 4$  for fcc structures. The (1 $\bar{1}$ 0) plane remains the plane of the same type in all three structures during this transformation.

The hexagonal transformation path connects, in the case of elemental solids, the bcc and hcp lattices and it differs qualitatively from the other two paths since it does not correspond to a homogeneous deformation. Instead, it is a combination of a homogeneous deformation that preserves the atomic volume, with a shuffling of alternate close-packed atomic planes in opposite directions. We interpolate linearly between the bcc and hcp structures in the directions [ $\bar{1}$ 10] and [001] and the shuffling is linearly coupled to the magnitude of straining in these directions. Therefore, we can use only a single parameter to describe this transformation path. Let us note that our path avoids the high-energy configurations that are encountered if only a shuffling or only a lattice deformation is applied, and is close to the minimum-energy path at constant volume. In our notation,  $p = 1$  corresponds to the bcc lattice and  $p = \sqrt{2}$  to the hcp lattice with ideal  $c/a$  ratio equal to  $\sqrt{8/3}$ . All other structures encountered along this path are orthorhombic. During the transformation the (110) plane of the bcc lattice becomes the (0001) plane of the hcp lattice. The bcc lattice is contracted along the [001] direction that converts into the [10 $\bar{1}$ ] direction in the hexagonal lattice, and extended along the [ $\bar{1}$ 10] direction which converts into [ $\bar{1}$ 2 $\bar{1}$ ] hcp direction. The exact relations characterizing this path are given in Ref. [32].

### 3. Results and discussion

#### 3.1. Tetragonal path

The total energy profiles along the tetragonal deformation path at experimental atomic volumes are shown in Fig. 1. In the region between the bcc and fcc structures, they are quite similar to those presented in Ref. [24]. However, we show the total energy profiles for a much wider interval of deformations and encounter three energy extrema along this path. Two of them, shown also in Ref. [24], correspond to the bcc ( $p = 1$ ) and fcc ( $p = \sqrt{2}$ ) structures and are dictated by the higher symmetry of these structures (all other structures along this path are tetragonal). The third extremum is located in the range of  $p > \sqrt{2}$  for Nb, Mo, Ta and W and of  $p < 1$  for Al and Cu. It is imposed by the energy increase when some atoms in the crystal move very close to each other under the deformation. For Cu, a very shallow minimum is located around  $p = 0.92$ , which is also found in some previous works [12,16,33]. The bcc phase in Al and Cu and the fcc phase in Nb, Mo, Ta and W are

unstable with respect to tetragonal deformation. The bct phase corresponding to the local minimum which is not dictated by the symmetry may be unstable. This has been discussed for the bct Cu phase in a recent paper [16]. Those authors found an energy decrease path which can bring the bct Cu phase to a lower energy body-centered orthorhombic phase.

We also investigated the minimum energy profiles along the tetragonal transformation path, where we relax the atomic volume to find the minimum total energy for each  $p$  (i.e. the  $cla$  ratio) along the path. In Fig. 2, we present the contour plot and the total energy profile along the minimum-energy path in Cu. The LDA calculations underestimate the equilibrium atomic volume for fcc Cu. Actually, we obtain a lattice constant of 3.52 Å for fcc Cu instead of an experimental value of 3.61 Å. Fig. 2b indicates that, for Cu, the total energy profile along the minimum-energy path is very similar to the constant-volume profile shown in Fig. 1, except that the energy difference between the bcc and fcc structures in the minimum-energy path is about 11 meV/atom greater than in the case of the constant (experimental)

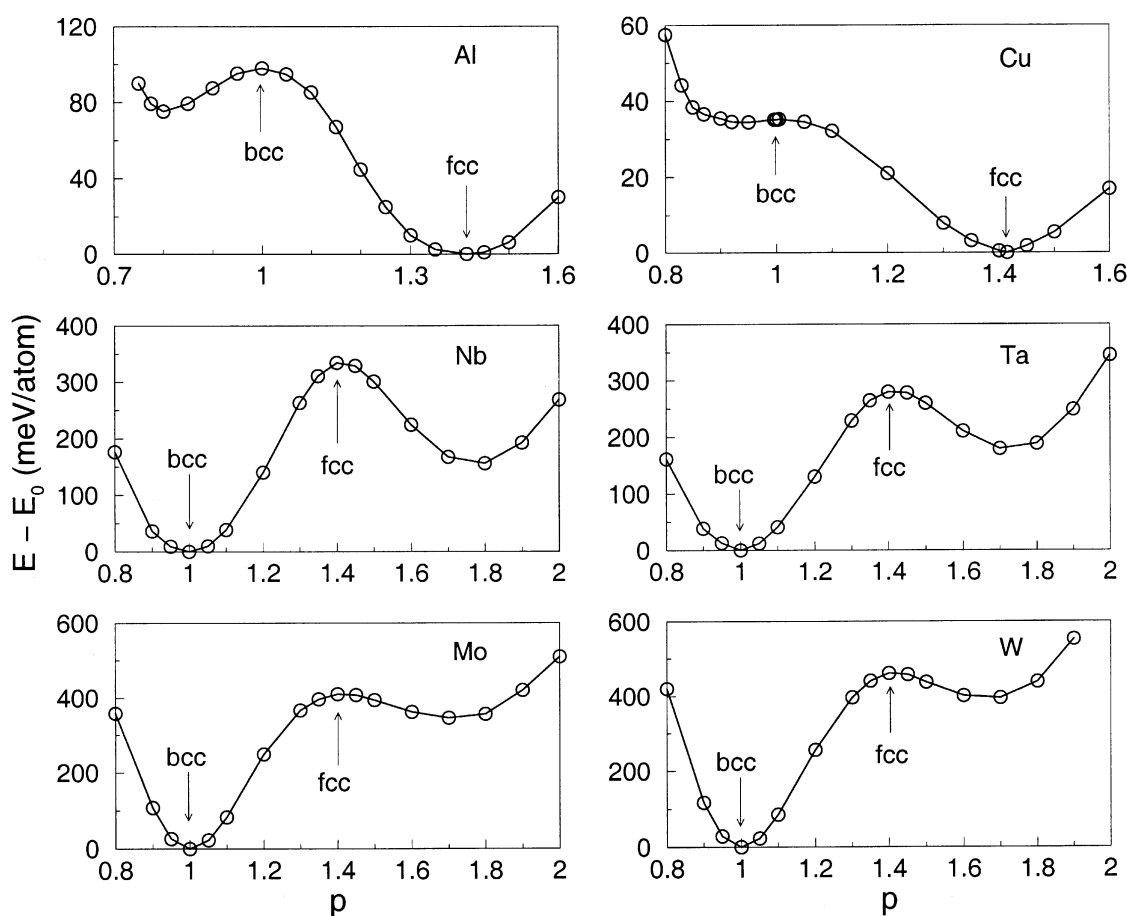


Fig. 1. Total energy per atom as a function of  $p$  along the tetragonal transformation path at the experimental atomic volume. Here  $E_0$  is the total energy of the ground-state structure.

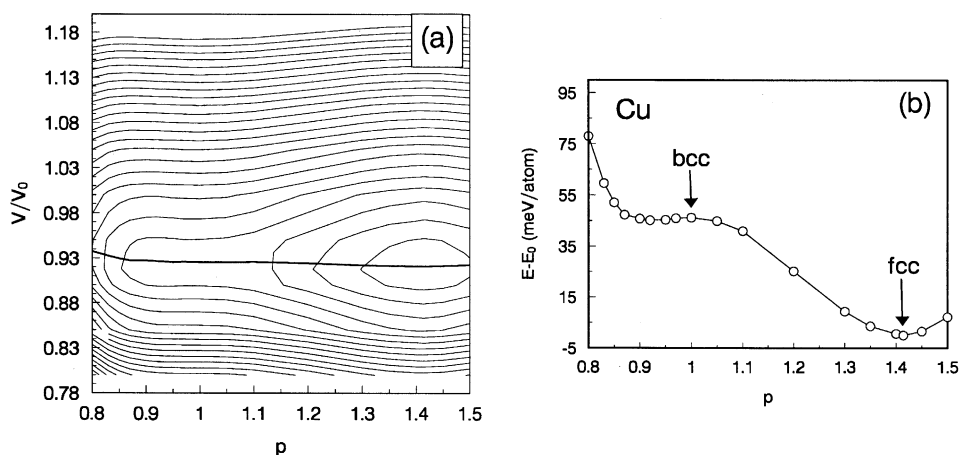


Fig. 2. (a) Total energy of Cu as a function of  $p$  and volume along the tetragonal transformation path.  $V_0$  is the experimental atomic volume. The thick solid line indicates the minimum-energy path. (b) The total energy profile along the minimum-energy path shown by the thick solid line in (a).

volume. Fig. 2 shows that the total energy as a function of volume and tetragonal deformation exhibits two minima (the ground-state fcc structure and the bct structure at  $p = 0.92$ ) and a saddle point at  $p = 1$  corresponding to the unstable bcc structure.

Our test calculations demonstrate that also in other metals studied here the total energy profiles along the minimum-energy path do not differ too much from those at (constant) experimental volume, similarly as in the case of Cu.

### 3.2. Trigonal path

In Fig. 3, we present the total energy profiles of studied metals along the trigonal transformation path. We can see that there are five extrema along the deformation path for Nb, Mo, and W, and three extrema for Al, Cu and Ta. As it is discussed above (Section 2), there exist three higher-symmetry structures along this path, i.e. bcc ( $p = 1$ ), sc ( $p = 2$ ) and fcc ( $p = 4$ ), and the energy extrema at these points are dictated by symmetry. In all cases, the sc structure corresponds to an energy maximum. For Nb, Mo and W, there exist two additional minima around the fcc structure. These local minima not corresponding to higher-symmetry structures have also been reported in previous works [26,33,34]. They are a direct consequence of the local maximum of total energy at the fcc and sc structures. In contrast to that, fcc Ta is stable against the trigonal deformation. This difference between fcc Ta and fcc Nb, Mo, and W is associated with the d-electron occupation and their density of states (DOS) at the Fermi energy. Actually, we find that the fcc Ta structure becomes unstable under pressures (for example  $V = 0.8 V_{eq}$ ), similar to those for Nb, Mo and W with the experimental atomic volumes. This is because pressures increase the electron occupation in the d band, and thus also change the DOS at the Fermi energy.

Again, if we allow the atomic volume to relax for each  $p$  (i.e. the  $c/a$  ratio) along the trigonal path, we find that the minimum energy profile has a similar feature as a constant-volume one. In Fig. 4, we present the contour plot and the minimum energy profile of Nb. We can see again that this profile is very similar to that given in Fig. 3, providing the same physical conclusions. Fcc and sc Nb correspond to a saddle point in Fig. 4a and are locally unstable with respect to trigonal deformation.

### 3.3. Hexagonal path

The results for Al, Ti, Nb, Mo, Ta and W along the hexagonal path are displayed in Fig. 5. Here we present the energy profile of Ti instead of Cu because Ti has a ground state of hcp. We see three energy extrema along this path. Two of them are dictated by the higher-symmetry structures (bcc at  $p = 1$  and hcp at  $p = \sqrt{2}$ ). Although hcp Al does not correspond to the ground state, it has a lower energy than the bcc phase and represents the lowest energy state along the path. We can see that all higher-energy phases (bcc Al and Ti, fcc Nb, Mo, Ta and W) are unstable. The third extremum (not dictated by symmetry) appears along the path similarly as in the case of the tetragonal path. Our results show that the orthorhombic Cu and Ti corresponding to the local minimum at  $p < 1$  in the hexagonal path have a lower energy than the bct Cu and Ti corresponding to the local minimum in the tetragonal path (Fig. 1). Fig. 6 shows the total energy results for Ti along the tetragonal and hexagonal paths. Also Cu in the orthorhombic structure has a lower energy than the bct structure; this is consistent with the finding by Jona and Marcus [16]. The orthorhombic structure of Ti corresponding to the local minimum in the hexagonal path is different from that one found by Vohra and Spencer in their high-pressure experiments [37] because in our case the orthorhombic structure is a distorted bcc structure, rather than a distorted hcp structure. In contrast,

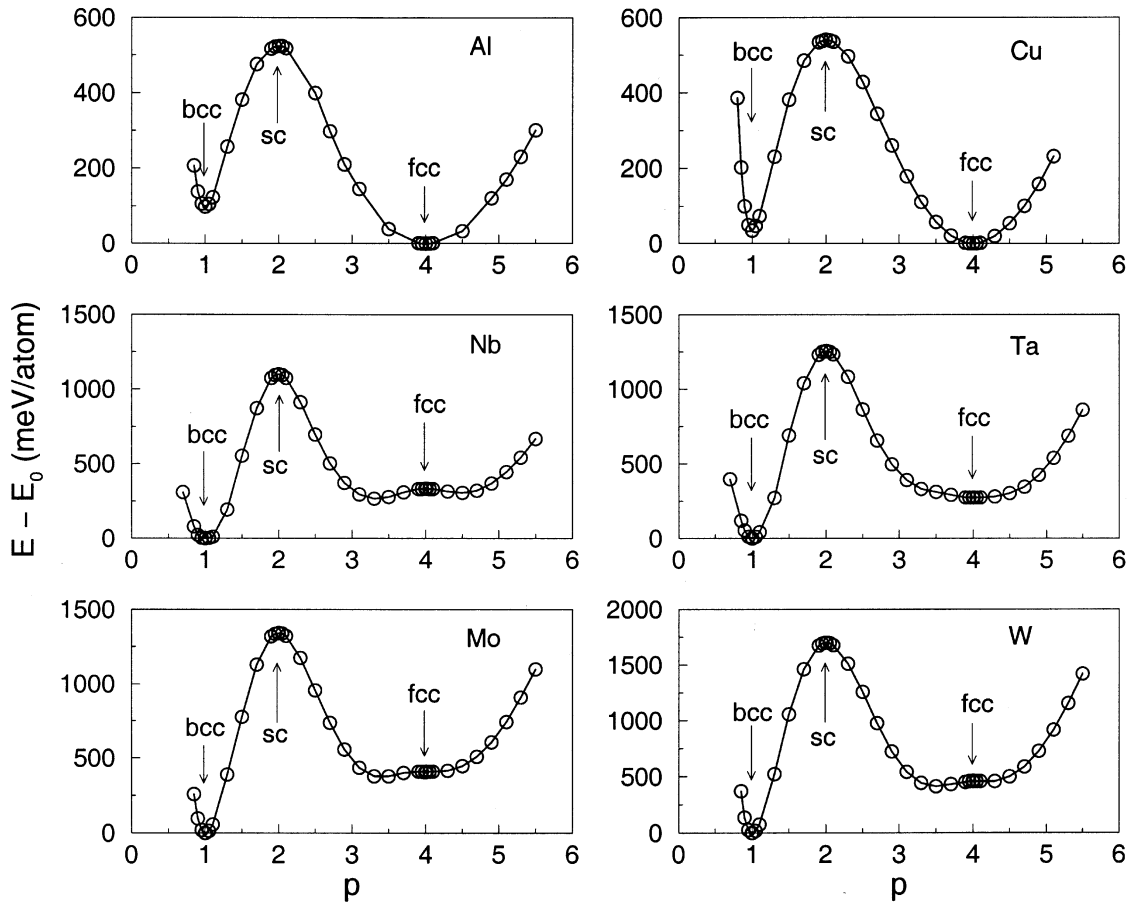


Fig. 3. Total energy per atom as a function of  $p$  along the trigonal transformation path at the experimental atomic volume. Here  $E_0$  represents the total energy of the ground-state structure.

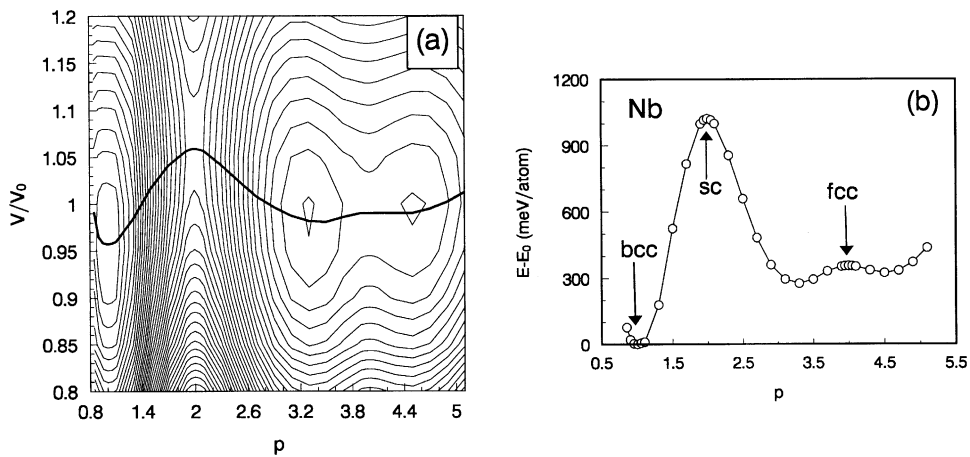


Fig. 4. (a) Total energy of Nb as a function of  $p$  and volume along the trigonal transformation path.  $V_0$  is the experimental atomic volume. The thick solid line indicates the minimum energy path. (b) The total energy profile along the minimum-energy path shown by the thick solid line in (a).

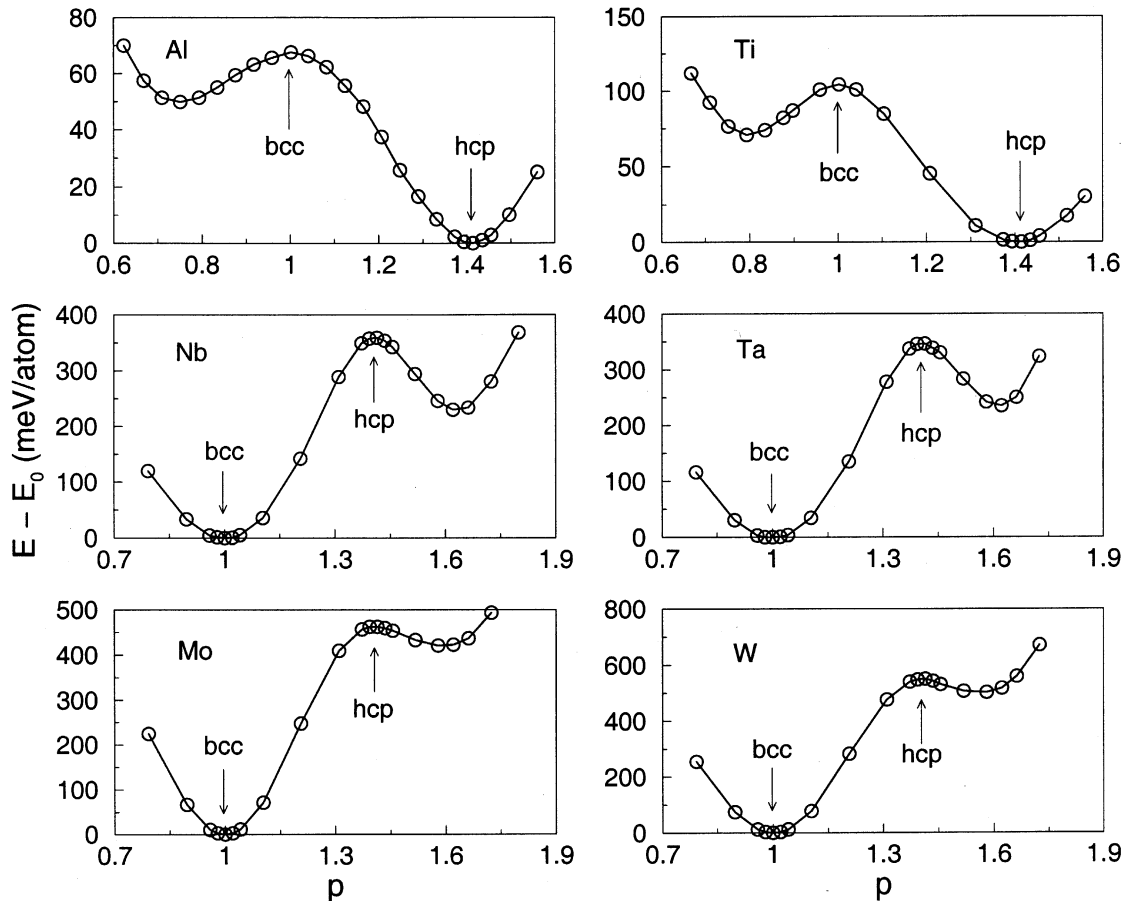


Fig. 5. Total energy per atom as a function of  $p$  along the hexagonal transformation path at the experimental atomic volume. Here  $E_0$  is the total energy of the ground-state structure (except for Al where it represents the lowest energy along the path).

we find that for Al, Nb, Mo, Ta and W the bct structure has a lower energy than the orthorhombic structure.

Let us note here that the energy profiles along the tetragonal and hexagonal path are very similar as the bcc structure is transformed into a close-packed structure (fcc or hcp) in both cases. The total energy difference between the hcp and fcc structures is quite small in all cases studied.

### 3.4. Elastic properties of higher-energy phases

Wills et al. [38] pointed out that the values of shear tetragonal modulus  $C' = (C_{11} - C_{12})/2$  for 5d cubic metals is roughly proportional to the absolute value of structural energy difference  $E_{\text{bcc}} - E_{\text{fcc}}$ . Subsequently, Craievich et al. [24] presented total energy profiles along the tetragonal (Bain's) deformation paths for all cubic 3d, 4d and 5d metals; from their fig. 1 (as well as from our Fig. 1) one can clearly see the above mentioned relation. It turns out that for all cubic 3d, 4d and 5d transition metals, if the ground state has the bcc structure, then the fcc structure is dynamically

(mechanically) unstable with respect to tetragonal deformation (i.e.  $C' < 0$ ), and if the ground state exhibits the fcc structure, then the bcc structure is dynamically unstable with respect to tetragonal deformation.

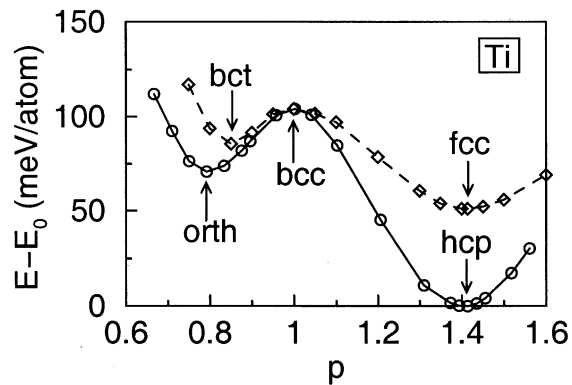


Fig. 6. Total energy as a function of  $p$  along the tetragonal and hexagonal transformation paths for Ti at the experimental atomic volume.  $E_0$  is the total energy of hcp Ti.

In addition, as pointed out by Grimvall [39], large and positive values of  $C'$  for either the bcc or fcc structure strongly correlate with the large and negative  $C'$  for the other structure. This relation is documented in Ref. [39] for cubic 5d metals and may be also seen in our data below. Grimvall [39] also discusses the behavior of trigonal shear modulus  $C_{44}$  in that series.

In Table 1, we present the values of elastic constants  $C'$  and  $C_{44}$  for all metals studied in this paper, i.e. for Al, Ti, Nb, Mo, Cu, Ta and W. We can see that all unstable structures of cubic metals exhibit  $C' < 0$  and, in addition to that, fcc Nb, Mo and W are dynamically unstable with respect to trigonal deformation ( $C_{44} < 0$ ). As stated by Grimvall [39],  $C_{44} < 0$  implies a more severe instability than  $C' < 0$  as the lattice is unstable under more deformation modes. This may be a reason why fcc Nb, Mo and W were not observed yet, whereas, for example, bcc Cu (with  $C' < 0$  and  $C_{44} > 0$ , Table 1) may be stabilized by external constraints at grain boundaries [33,48] or as a thin film on some substrates [1–8], as discussed below. In case of Ti, the fcc structure is quite close to the hcp ground state structure ( $E_{\text{fcc}} - E_{\text{hcp}} = 51$  meV/atom) and is stable with respect to tetragonal and trigonal deformation ( $C' > 0$ ,  $C_{44} > 0$ ; Fig. 6). On the other hand, bcc Ti is dynamically unstable with respect to tetragonal deformation.

Grimvall [39,40] concludes that when either the bcc or fcc structure is dynamically unstable, there are large discrepancies between the semiempirical enthalpy differences  $H_{\text{bcc}} - H_{\text{fcc}}$  obtained from the CALPHAD method and ab initio results. However, as we can see from the above discussion, this is the case of most transition metals. In the ab initio calculation, the dynamical instability is suppressed as we assume a rigid lattice (which, in reality, might be stabilized by some external constraints), and the energy and enthalpy of such a structure have a well defined physical meaning. However, in our opinion, it is still not clear how

such values may be compared with those obtained from semiempirical CALPHAD method.

### 3.5. Stability of higher-energy phases in pseudomorphic films

As mentioned in Section 1, some higher-energy phases can be stabilized experimentally in pseudomorphic films. Sometimes the films have a nearly ideal cubic structure. For example, Cu{001} films on Fe{001}/Ag{001} were found to have a nearly perfect bcc structure [7] and a slightly distorted bcc Cu structure was observed in Cu/Nb multilayered films [8]. However, as shown in this work and in Refs. [24,26], free-standing higher-energy phases are unstable. Previous studies [24,42,43] argued that the entropy contribution to the free energy are responsible for the stability of (free-standing) higher-energy phases at high temperatures. However, the existence of higher-energy phases in pseudomorphic films cannot be explained by this mechanism because the phases are usually observed at low temperatures, such as at room temperature. Now the problem is how we can understand the stability of higher-energy phases occurring in pseudomorphic films.

Heteroepitaxial growth is extremely complicated because both thermodynamics and kinetics play a role here [44–46]. Heteroepitaxial films or multilayers also are not usually in their equilibrium state. However, for some cases, such as bcc Cu precipitates in a bcc Fe matrix [47] and the bcc Cu phase in certain Cu grain boundaries [48], thermodynamics may play a key role. In the following we will discuss the stability of higher-energy phases in pseudomorphic films from the point of view of thermodynamics. Assuming a bcc Cu film on the Fe{001} substrate, we can see that the bcc Cu which is dynamically (mechanically) unstable with respect to tetragonal deformation ( $C' < 0$ ) can be stabilized by the substrate epitaxial constraint. Let us note that  $C_{44}$  of the bcc Cu exhibits a positive value of

Table 1

Elastic constants  $C'$  and  $C_{44}$  for the elements studied in this paper are determined from the curves in Figs. 1 and 3. The experimental values (exp.) are compiled from Ref. [41]

Element	structure at 0 K		bcc $C'$ (GPa)	bcc $C_{44}$ (GPa)	fcc $C'$ (GPa)	fcc $C_{44}$ (GPa)
Al	fcc	Calc.	–16	46	25	39
		Exp.			26	31
Ti	hcp	Calc.	–15	39	20	50
Cu	fcc	Calc.	–6	112	27	82
		Exp.			23	76
Nb	bcc	Calc.	53	24	–152	–57
		Exp.	56	29		
Mo	bcc	Calc.	132	120	–88	–7
		Exp.	157	109		
Ta	bcc	Calc.	61	73	–102	19
		Exp.	52	85		
W	bcc	Calc.	173	152	–142	–60
		Exp.	163	163		

112 GPa ([33], Table 1). We will show below how the substrate prevents the instability corresponding to sliding of bcc Cu {110} atomic planes (this instability is due to the negative  $C'$  of bcc Cu).

Let us suppose that we have a supercell with  $n$  Cu atoms and  $n$  Fe atoms, which is used to simulate a bcc Cu film on the bcc Fe {001} substrate (Usually in a supercell model a certain thickness of the substrate material is used to simulate the substrate. Since the substrate is usually assumed sufficiently thick or infinite we may take the substrate thicker than the film. In the present example we assume that the substrate has a same thickness of the film). The total energy of such a supercell (per atom) can be roughly described as  $(E_{\text{Cu}} + E_{\text{Fe}})/2$ , where  $E_{\text{Cu}}$  and  $E_{\text{Fe}}$  are the total energies (per atom) of bcc Cu (having an experimental atomic volume of bcc Fe) and of bcc Fe, respectively. The approximated total energies for the supercell, as well the total energies of bcc Cu and bcc Fe, are presented in Fig. 7. The difference between a real supercell calculation and  $(E_{\text{Cu}} + E_{\text{Fe}})/2$  is the surface energy plus the interface energy. For Fe we take its ferromagnetic (FM) state because FM bcc Fe is stable with respect to the tetragonal distortion, whereas its nonmagnetic state is unstable along this path [49]. We also employ the LDA exchange–correlation functional for ferromagnetic Fe in our calculations. Although it is well known that LDA can predict a wrong ground state of Fe [50], the present stability analysis is not affected by employing the LDA exchange–correlation functional because both LDA and GGA give a similar dependence of total energy on the deformation in the neighborhood of the bcc phase along the tetragonal path [49].

From Fig. 7 it is very clear that the complex system of the film and the substrate, modeled by a supercell, is stable and has a positive value of  $C'$ . In this example we do not invoke

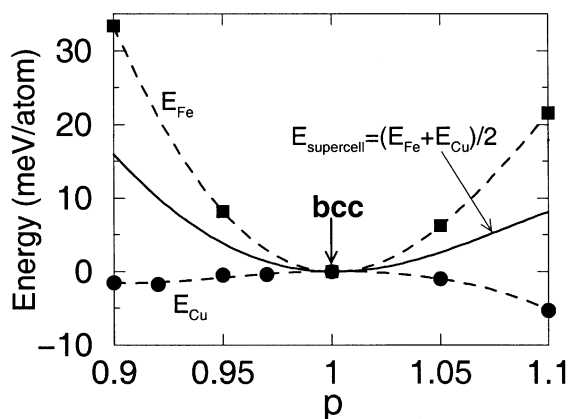


Fig. 7. Total energies of tetragonally deformed bcc Cu and bcc ferromagnetic Fe as a function of  $p$  along the tetragonal transformation path in the neighborhood of the bcc structure. The solid line is the approximate total energy of the supercell simulating a Cu film on the Fe substrate.

any contributions from the surface and interface. Actually, experiments [8] have also shown that the bcc Cu phase can be stabilized in the Cu/Nb multilayered system. This indicates that the film free surface is not necessary in order to stabilize the bcc Cu phase. Therefore, we argue that the stability of higher-energy phases in pseudomorphic films is due to the bulk stability of the substrate material. However, by this argument we do not mean that a film (including an unstable higher-energy phase) can always be stabilized by any stable substrate, and that surface and interface effects can be underestimated. Actually, in order to stabilize a film including an unstable higher-energy phase, a coherent film has to be formed, which is determined by the geometric factors and properties of both substrate and film materials, such as the free enthalpies of the substrate surface, the film surface and the interface between the film and the substrate.

The constraint mechanism is compatible with the experimental observation [8] that for thicker films the higher-energy phase transforms back to the ground state. For a thick film, the layers far away from the interface tend to have equilibrium bulk lattice constants of the film material at its ground state. We can consider this as a driving force to drive a thick film back to its ground state. This driving force becomes stronger and stronger with increasing film thickness. Therefore, a sufficiently thick film will have the ground state structure.

#### 4. Summary

We have performed full-potential first-principles electronic structure calculations for some simple and transition metals along the tetragonal, trigonal and hexagonal transformation paths. We find that there are some energy extrema in the total energy profiles which are not dictated by the symmetry. However, a higher-symmetry structure encountered along the transformation paths always corresponds to an extremum of the total energy. The higher-energy phases, such as bcc Al, Cu and Ti and fcc Nb, Mo, Ta and W, are found to be unstable. In contrast, some higher-energy phases are observed experimentally in pseudomorphic films. We also have explained the stability of these higher-energy phases in pseudomorphic films in terms of the epitaxial constraint of the substrate.

#### Acknowledgements

This research was supported by the Grant Agency of the Academy of Sciences of the Czech Republic (Project No. A1010817), by the Grant Agency of the Czech Republic (Project No. 106/02/0877), by the Research Project Z2041904 of the Academy of Sciences of the Czech Republic, by Oak Ridge National Laboratory, managed by

UT-Battell, LLC, for the US Department of Energy, and by NSF (Grant No. DMR-0071893). A part of this study has been performed in the framework of the Project COST OC 523.90. The use of the computer facility at the MetaCenter of the Masaryk University, Brno is acknowledged. We also thank G. Grimvall for discussion and for delivering the manuscript of the paper [39] before its publication.

## References

- [1] M.H. Kang, R.C. Tatar, E.J. Mele, P. Soven, Real-space formulation of the mixed-basis pseudopotential method: bulk structural properties of elemental copper, *Phys. Rev. B* 35 (1987) 5457–5472.
- [2] I.A. Morrison, M.H. Kang, E.J. Mele, First-principles determination of the bulk phase diagram for body-centered-tetragonal copper: application to epitaxial growth of Cu on Fe{100}, *Phys. Rev. B* 39 (1989) 1575–1580.
- [3] H. Li, S.C. Wu, D. Tian, J. Quinn, Y.S. Li, F. Jona, P.M. Marcus, Epitaxial growth of body-centered-tetragonal copper, *Phys. Rev. B* 40 (1989) 5841–5844.
- [4] H. Liu, D. Tian, J. Quinn, Y.S. Li, F. Jona, P.M. Marcus, Low-energy electron diffraction and photoemission study of epitaxial films of Cu on Ag{001}, *Phys. Rev. B* 43 (1991) 6342–6346.
- [5] T. Kraft, P.M. Marcus, M. Methfessel, M. Scheffler, Elastic constants of Cu and the instability of its bcc structure, *Phys. Rev. B* 48 (1993) 5886–5890.
- [6] E.H. Hahn, E. Kampshoff, N. Wälchli, K. Kern, Strain driven fcc–bcc phase transition of pseudomorphic Cu films on Pd(100), *Phys. Rev. Lett.* 74 (1995) 1803–1806.
- [7] B. Heinrich, Z. Celinski, J.F. Cochran, W.B. Muir, J. Rudd, Q.M. Zhong, A.S. Arrott, K. Myrtle, Ferromagnetic and antiferromagnetic exchange coupling in bcc epitaxial ultrathin Fe(001)/Cu(001)Fe(001) trilayers, *Phys. Rev. Lett.* 64 (1990) 673–676.
- [8] H. Kung, Y.-C. Lu, A.J. Griffin Jr., M. Nastasi, T.E. Mitchell, J.D. Embury, Observation of body centered cubic Cu in Cu/Nb nanolayered composites, *Appl. Phys. Lett.* 71 (1997) 2103–2105.
- [9] T.E. Mitchell, Y.-C. Lu, A.J. Griffin Jr., M. Nastasi, H. Kung, Microstructure/properties relations of advanced materials structure and mechanical properties of copper/niobium multilayers, *J. Am. Ceram. Soc.* 80 (1997) 1673–1676.
- [10] H. Geng, J.W. Heckman, W.P. Pratt, J. Bass, F.J. Espinosa, D. Lederman, M.A. Crimp, Occasional long-range nonequilibrium body-centered-cubic structures in NiFe/Cu spin valves, *J. Appl. Phys.* 86 (1999) 4166–4175.
- [11] Y.S. Li, J. Quinn, H. Li, D. Tian, F. Jona, P.M. Marcus, Large strains in the epitaxy of Cu on Pt{001}, *Phys. Rev. B* 44 (1991) 8261–8266.
- [12] S. Jeong, Structural properties of bulk copper: pseudopotential plane-wave-basis study, *Phys. Rev. B* 53 (1996) 13973–13976.
- [13] Ch. Rath, J.E. Prieto, S. Müller, R. Miranda, K. Heinz, hcp-to-fcc stacking switch in thin cobalt films induced by Cu capping, *Phys. Rev. B* 55 (1997) 10791–10799.
- [14] E. Abe, T. Kumagai, M. Nakamura, New ordered structure of TiAl studied by high-resolution electron microscopy, *Intermetallics* 4 (1996) 327–333.
- [15] P.M. Marcus, F. Jona, Identification of metastable phases: face-centred cubic Ti, *J. Phys.: Condens. Matter* 9 (1997) 6241–6246.
- [16] F. Jona, P.M. Marcus, Structural properties of copper, *Phys. Rev. B* 63 (2001) 094113-1–094113-8.
- [17] P. Hohenberg, W. Kohn, Structural properties of copper, *Phys. Rev.* 136 (1964) B864–B871.
- [18] W. Kohn, L.J. Sham, Self-consistent equations including exchange and correlation effects, *Phys. Rev.* 140 (1965) A1133–A1138.
- [19] G.W. Fernando, R.E. Watson, M. Weinert, Y.J. Wang, J.W. Davenport, Cohesion and lattice stabilities in the 5d transition metals: full versus muffin-tin potentials, *Phys. Rev. B* 41 (1990) 11813–11821.
- [20] Y.Y. Ye, Y. Chen, K.M. Ho, B.N. Harmon, P.A. Lindgard, Phonon–phonon coupling and the stability of the high-temperature bcc phase of Zr, *Phys. Rev. Lett.* 58 (1987) 1769–1772.
- [21] D. Nguyen Manh, A.M. Bratkovsky, D.G. Pettifor, Quantum mechanical predictions in intermetallics modelling, *Philos. Trans. R. Soc. London A* 351 (1995) 529–542.
- [22] L. Cortella, B. Vinet, P.J. Desré, A. Pasturel, A.T. Paxton, M. von Schilfgarde, Evidences of transitory metastable phases in refractory metals solidified from highly undercooled liquids in a drop tube, *Phys. Rev. Lett.* 70 (1993) 1469–1472.
- [23] V. Ozoliņš, C. Wolverton, A. Zunger, Effects of anharmonic strain on the phase stability of epitaxial films and superlattices: applications to noble metals, *Phys. Rev. B* 57 (1998) 4816–4828.
- [24] P.J. Craievich, M. Weinert, J.M. Sanchez, R.E. Watson, Local stability of nonequilibrium phases, *Phys. Rev. Lett.* 72 (1994) 3076–3079.
- [25] P.J. Craievich, J.M. Sanchez, R.E. Watson, M. Weinert, Structural instabilities of excited phases, *Phys. Rev. B* 55 (1997) 787–797.
- [26] M. Šob, L.G. Wang, V. Vitek, Local stability of higher-energy phases in metallic materials and its relation to the structure of extended defects, *Comput. Mater. Sci.* 8 (1997) 100–106.
- [27] V.L. Sliwko, P. Mohn, K. Schwarz, P. Blaha, The fcc–bcc structural transition: I. A band theoretical study for Li, K, Rb, Ca, Sr, and the transition metals Ti and V, *J. Phys.: Condens. Matter* 8 (1996) 799–816.
- [28] P. Blaha, K. Schwarz, J. Luitz, Computer code WIEN97, Vienna University of Technology, 1997, Improved and updated Unix version of the original copyrighted WIEN code, P. Blaha, K. Schwarz, P. Sorantin, S.B. Trickey, Full-potential, linearized augmented plane wave programs for crystalline systems, *Comput. Phys. Commun.* 59 (1990) 399–415.
- [29] J.P. Perdew, Y. Wang, Accurate and simple analytic representation of the electron-gas correlation energy, *Phys. Rev. B* 45 (1992) 13244–13249.
- [30] D.M. Ceperly, B.J. Alder, Ground state of the electron gas by a stochastic method, *Phys. Rev. Lett.* 45 (1980) 566–569.
- [31] R.M. Wentzcovitch, M.L. Cohen, Theoretical model for the hcp–bcc transition in Mg, *Phys. Rev. B* 37 (1988) 5571–5576.

- [32] V. Paidar, L.G. Wang, M. Šob, V. Vitek, A study of the applicability of many-body central force potentials in NiAl and TiAl, *Model. Simul. Mater. Sci. Engng* 7 (1999) 369–381.
- [33] L.G. Wang, M. Šob, Structural stability of higher-energy phases and its relation to the atomic configurations of extended defects: the example of Cu, *Phys. Rev. B* 60 (1999) 844–850.
- [34] M.J. Mehl, D.A. Papaconstantopoulos, Applications of a tight-binding total-energy method for transition and noble metals: elastic constants, vacancies, and surfaces of monoatomic metals, *Phys. Rev. B* 54 (1996) 4519–4530.
- [35] Y. Mishin, M.J. Mehl, D.A. Papaconstantopoulos, A.F. Voter, J.D. Kress, Structural stability and lattice defects in copper: ab initio, tight-binding, and embedded-atom calculations, *Phys. Rev. B* 63 (2001) 224106-1–224106-16.
- [36] Y. Mishin, D. Farkas, J. Mehl, D.A. Papaconstantopoulos, Interatomic potentials for monoatomic metals from experimental data and ab initio calculations, *Phys. Rev. B* 59 (1999) 3393–3407.
- [37] Y.K. Vohra, P.T. Spencer, Novel  $\gamma$ -phase of titanium metal at megabar pressures, *Phys. Rev. Lett.* 86 (2001) 3068–3071.
- [38] J.M. Wills, O. Eriksson, P. Söderlind, A.M. Boring, Trends of the elastic constants of cubic transition metals, *Phys. Rev. Lett.* 68 (1992) 2802–2805.
- [39] G. Grimvall, Variation of elastic shear constants in transition metal alloys, *Proceedings of Third International Alloy Conference: An Interdisciplinary Approach to the Science of Alloys in Metals, Minerals and Other Materials Systems*, June 30–July 5, 2002, Estoril/Cascais, Portugal, to be published.
- [40] G. Grimvall, Reconciling ab initio and semiempirical approaches to lattice stabilities, *Ber. Bunsenges. Phys. Chem.* 102 (1998) 1083–1087.
- [41] G. Simmons, H. Wang, *Single Crystal Elastic Constants and Calculated Aggregate Properties: A Handbook*, 2nd ed., MIT Press, Cambridge, MA, 1971.
- [42] A. Fernández Guillermet, V. Ozoliņš, G. Grimvall, M. Körling, Phase stabilities in the Pt–W system: thermodynamic and electronic-structure calculations, *Phys. Rev. B* 51 (1995) 10364–10374.
- [43] E.G. Moroni, G. Grimvall, T. Jarlborg, Free energy contributions to the hcp–bcc transformation in transition metals, *Phys. Rev. Lett.* 76 (1996) 2758–2761.
- [44] Z.Y. Zhang, Q. Niu, C.-K. Shih, Electronic growth of metallic overlayers on semiconductor substrates, *Phys. Rev. Lett.* 80 (1998) 5381–5384.
- [45] Z.Y. Zhang, M.G. Lagally, Atomistic processes in the early stages of thin-film growth, *Science* 276 (1997) 377–383.
- [46] C.W. Snyder, B.G. Orr, H. Munekata, Effect of surface tension on the growth mode of highly strained InGaAs on GaAs(100), *Appl. Phys. Lett.* 62 (1993) 46–48.
- [47] S.R. Goodman, S.S. Brenner, J.R. Low, An FIM-atom probe study of the precipitation of copper from iron-1.4 at. pct copper: I. Field-ion microscopy, *Metall. Trans.* 4 (1973) 2363–2369.
- [48] C. Schmidt, F. Ernst, M.W. Finnis, V. Vitek, Prediction and observation of the bcc structure in pure copper at a  $\Sigma$  3 grain boundary, *Phys. Rev. Lett.* 75 (1995) 2160–2163.
- [49] M. Friák, M. Šob, V. Vitek, Ab initio calculation of phase boundaries in iron along the bcc–fcc transformation path and magnetism of iron overlayers, *Phys. Rev. B* 63 (2001) 052405-1–052405-4.
- [50] C.S. Wang, B.M. Klein, H. Krakauer, Theory of magnetic and structural ordering in iron, *Phys. Rev. Lett.* 54 (1985) 1852–1855.